INTERNATIONAL JOURNAL OF NUMERICAL MODELLING: ELECTRONIC NETWORKS, DEVICES AND FIELDS
Int. J. Numer. Model. 2006; **19**:215–228
Published online in Wiley InterScience (www.interscience.wiley.com). DOI: 10.1002/jnm.607

Off-normal incidence simulations of metamaterials using FDTD

D. Schurig*,†

Department of ECE, Duke University, Box 90291, Durham, NC 27708, U.S.A.

SUMMARY

A method is described for applying FDTD simulation to electromagnetic metamaterial slabs with off-normal incident plane wave radiation. Issues of incommensurate spatial periods and interpolation of irregularly spaced data are discussed. Validity of the method is tested on a dielectric slab with known analytical solutions and the method is used to analyse split ring resonators of current interest. Copyright © 2006 John Wiley & Sons, Ltd.

KEY WORDS: off-normal; simulation; FDTD; metamaterials

1. INTRODUCTION

The field of electromagnetic metamaterials has experienced significant growth in its theoretical development, range of material operation, and potential for applications. Strong electromagnetic response has been seen in the Terahertz frequency range [1, 2]. The understanding of negative material response has been extended from isotropic to anisotropic (indefinite) [3] to chiral and bianisotropic [4, 5]. Application enabling developments have emerged including improved microwave devices [6], realization of super lensing [7], and reduced optical aberrations of curved lenses [8]. Implementing these developments requires numerical simulation of metamaterials at the unit cell level. Since analytical calculation of the response of an arbitrary composite material is typically intractable, numerical simulation is the standard method for metamaterial design, and is also necessary for the interpretation of complex experimental reflection and transmission data.

Methods for simulating the reflection and transmission coefficients (S parameters) at normal incidence are well established using both commercial and custom software [9–11]. These

*Correspondence to: D. Schurig, Department of ECE, Duke University, Box 90291, Durham, NC 27708, U.S.A.
†E-mail: dschurig@duke.edu

Contract/grant sponsor: IC Postdoctoral Research Fellowship Program
Contract/grant sponsor: Naval Air Warfare Center Weapons Division; contract/grant number: N68936-05-C-0011

 Accepted 29 December 2005

simulations are used to extract the effective medium properties of the materials, ε and μ. These effective medium properties can, in theory, be used to predict the response of an arbitrary shape of the material, to radiation incident at any angle. However, there are cases where this response extrapolation using effective medium theory is questionable, and a direct simulation of off-normal incidence response would be desirable. For example, it is often not easy to satisfy the effective medium limit,

$$ka \ll 1 \tag{1}$$

due to design or manufacturing limitations. This is the case for many of the samples fabricated in the literature where $ka \sim 1$, (e.g. Reference [12]). Another example is a thin structure of single unit cell thickness. Such a structure may not be considered a volumetric material describable by volumetric material properties. In this case, it is even unclear how to define the lattice parameter in the thin direction. This issue has arisen in research of high-frequency metamaterials where fabrication of single layers of in-plane structures is relatively straightforward, but assembly of multiple layers, into a volumetric sample is difficult [1, 2]. Even when assembly is possible, it may be desirable to measure individual layers of material prior to assembling a costly sample. Additionally, single layer, in plane structures may not be testable by normally incident radiation. For example, radiation normally incident on in-plane split ring resonators will not yield any excitation flux threading the rings.

Off-normal incidence simulations of metamaterials are not well developed in the literature, but can be accomplished with commercial software using an appropriate mapping of the problem, and interpolation of the simulation data. For the simulations to be presented here, we use Microwave Studio (MWS) from CST corporation. The resulting simulation data can be processed, interpolated and plotted using many standard packages, but the process will be easier if advanced interpolation algorithms, such as Delauney triangulation, are available.

The mapping we will use to convert a free space problem to a bounded simulation is sometimes called the *waveguide simulator* method. This method, which predates modern numerical modelling, was originally an experimental technique [13]. More recently, the photonic crystal community has used this and other techniques for reflection calculations [14–16].

2. BOUNDARIES AND FIELDS

Electromagnetic simulation software can solve for the fields inside a rectangular volume containing arbitrary material objects. Each face of this volume is configured with a boundary condition, usually electric, magnetic or open. The electric boundary condition forces electric fields parallel to the surface to be zero, as would be the case at a perfectly conducting surface. Analogously, the magnetic boundary condition forces magnetic fields parallel to the surface to be zero. The open boundary condition simulates a reflectionless, impedance matched surface, equivalent to the surface of an infinite half space.

Faces assigned the open condition can be configured as ports for radiation entering or exiting the volume. This provides a means of exciting the volume and measuring the response. The software will automatically determine the modes of these ports. For example, if two *pairs* of opposite faces are set to the electric boundary condition, and the remaining pair of opposite faces is set to open, then the modes of ports configured on the open faces would be the well-known modes of a metallic walled rectangular wave guide [17].

The simulation software will excite a specified port with a specified mode pattern of entering radiation, determine the fields inside the volume, and decompose the radiation exiting all the ports into exiting modes. This decomposition yields a set of complex amplitudes of the exiting modes relative to the entering mode. These complex amplitudes are the S parameters, $S_{i(m)j(n)}$, where m is the mode and i is the port through which radiation is exiting, and n is the mode and j is the port that is providing the excitation.

If one pair of opposite faces is electric and one pair is magnetic we can simulate TEM plane waves. Specifically, the modes of this TEM waveguide are pairs of plane waves with equal and opposite angles of propagation relative to the waveguide axis. Below, we will analyse a sum of two plane waves and demonstrate that there are nodal surfaces that match these boundary conditions. We will choose the electric pair of faces to be y oriented, the magnetic pair to be x oriented and the open pair to be z oriented, (Figure 1). First we note that a TEM plane wave propagating in the z-direction (i.e. normally incident) with electric field polarized in the y-direction will match the boundary conditions. This mode can propagate at any frequency and will thus be the lowest mode, since the modes are typically ordered by their low-frequency cut-off. For higher-order modes, we start with a pair of plane waves polarized with electric field in the y-direction, propagating at angle θ to the z-axis,

$$\mathbf{E} = \hat{\mathbf{y}}\mathrm{e}^{\mathrm{i}\mathbf{k}_+\cdot\mathbf{r}} + \hat{\mathbf{y}}\mathrm{e}^{\mathrm{i}\mathbf{k}_-\cdot\mathbf{r}} \tag{2}$$

where the wave vectors are given by

$$\mathbf{k}_\pm = \pm k_x\hat{\mathbf{x}} + k_z\hat{\mathbf{z}} \tag{3}$$

and the wave vector components by

$$k_x = \sin\theta\frac{\omega}{c} \quad \text{and} \quad k_z = \cos\theta\frac{\omega}{c} \tag{4}$$

The electric field can then be written as

$$\mathbf{E} = 2\hat{\mathbf{y}}\cos(k_x x)\mathrm{e}^{\mathrm{i}k_z z} \tag{5}$$

The electric boundary conditions are obviously satisfied.

Using Maxwell's equation,

$$\nabla \times \mathbf{E} = \mathrm{i}\omega\mu\mathbf{H} \tag{6}$$

we find the magnetic field,

$$\mathbf{H} = \frac{2}{\omega\mu}[-\hat{\mathbf{x}}k_z\cos(k_x x) + \hat{\mathbf{z}}\mathrm{i}k_x\sin(k_x x)]\mathrm{e}^{\mathrm{i}k_z z} \tag{7}$$

We can see that on x-planes specified by

$$k_x x = m\pi \tag{8}$$

the z-component of magnetic field is zero and the field would satisfy a magnetic boundary condition. If the simulation volume has a length in the x-direction given by l_x, then allowed values for k_x are

$$k_x = \sin\theta\frac{\omega}{c} = \frac{m\pi}{l_x} \tag{9}$$

Now we see that by choosing the mode number, m, and the length of the simulation volume in the x-direction, l_x, we can set the angle of the plane waves. If we want to find the reflection and

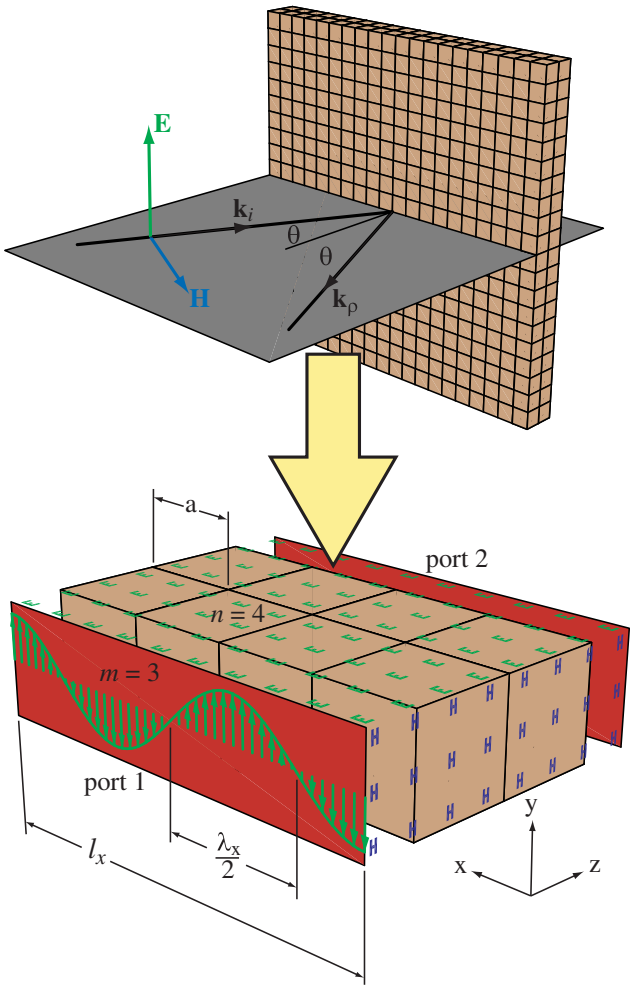

Figure 1. Converting a large (or infinite) model to a finite simulation volume space with appropriate port modes and boundary conditions.

transmission coefficient of a plane wave for a particular angle of incidence we simulate with an appropriate choice of simulation volume and mode.

$$\rho(\theta) = S_{1(m)1(m)} \tag{10}$$

$$\tau(\theta) = S_{2(m)1(m)} \tag{11}$$

The fields we have chosen here correspond to *S*-polarization in free space jargon and *TE* modes in wave guide jargon. We could just as easily have started with,

$$\mathbf{H} = \hat{\mathbf{x}} e^{i\mathbf{k}_+ \cdot \mathbf{r}} + \hat{\mathbf{x}} e^{i\mathbf{k}_- \cdot \mathbf{r}} \tag{12}$$

to obtain results for *P*-polarization with *TM* modes.

As mentioned above, the simulation software orders the modes by cut-off frequency. A given mode is cut-off when the equivalent conditions apply: $k_z = 0$, $k_x = \omega/c$ and $\theta = \pi/2$. From (9), the cut-off frequency of a mode is given by

$$f_c = \frac{mc}{2l_x} \tag{13}$$

and the mode will not propagate (i.e. k_z is imaginary) below this frequency.

3. THE f-sin θ PARAMETER SPACE

FDTD simulations give S-parameter results at a set of evenly spaced frequency points. These points are obtained by taking a discrete Fourier transform of the transient response of the system to an excitation pulse. The pulse is chosen to have significant amplitude over the range of frequencies where results are desired. The upper frequency of the pulse determines the mesh density required. The lower frequency may be set greater than zero to prevent the excitation of certain modes of the volume or ports. For example, stimulation of a port mode below its cut-off may excite surface modes with large amplitudes that swamp the desired propagating results.

A significant issue with off-normal FDTD is that the incident angle will not be constant over the range of frequencies that the simulation provides. We can see this from (9) and (13) which yield

$$f \sin\theta = f_c \tag{14}$$

The cut-off frequency, f_c, is fixed in the simulation by the choice of mode and the dimensions of the simulation volume. The sine of the angle of incidence will be inversely related to the frequency at each of the frequency points provided by the simulation. This set of points will lie on a hyperbola in the f-sin θ parameter space. Of course, one can cover any desired region of this parameter space with an appropriate set of hyperbolas obtained from separate simulations with different modes, m, and lengths, l_x, Figure 2. The intercept of the hyperbola with the line, $\sin\theta = 1$, yields the cut-off frequency for the mode. As seen from the figure a set of simulations with uniformly spaced cut-off frequencies gives a reasonably uniform coverage of the entire parameter space, with hyperbolic curves, except near the origin.

Our goal may then be to run a set of simulations with uniformly spaced cut-off frequencies that cover the region of f-sin θ parameter space of interest,

$$f_i = i\Delta f \tag{15}$$

where f_i are cut-off frequencies spaced Δf apart and indexed by i. For metamaterials this will not, in general, be possible, because the simulation volume must be composed of an integral number of finite size unit cells. Thus, it is required that

$$l_x = na \tag{16}$$

with a, the unit cell size, and n, the number of unit cells, in the x-direction. (Since the response of a partial unit cell is not useful for predicting material behaviour, n must be an integer.) From (13) and (16) we find

$$f_c = \frac{c}{2a}\frac{m}{n} \tag{17}$$

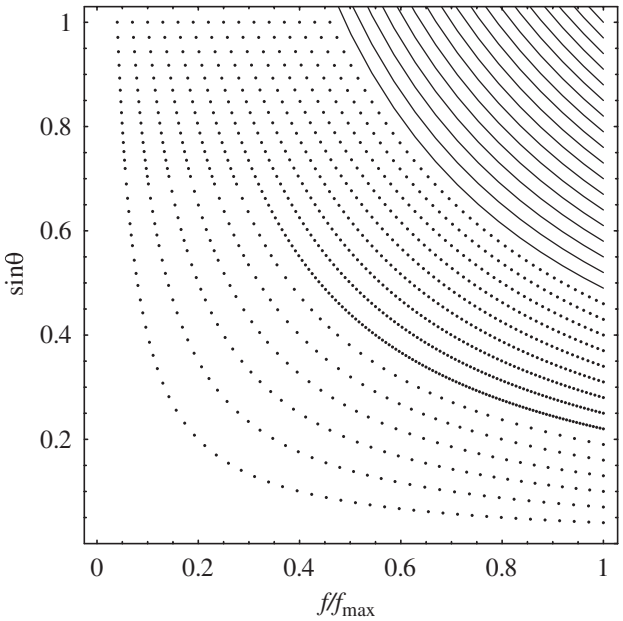

Figure 2. The parameter space of frequency and angle of incidence. A single simulation gives results along a hyperbolic curve in this space. In the upper right these hyperbolic curves are shown solid. In the middle range, individual points along the curves are shown evenly spaced in frequency. The lower curves have undergone a thinning procedure the yields more uniform point distribution in this parameter space.

so that the cut-off frequency is a product of fixed constants, and a ratio of integers. We can still find a set of approximately evenly spaced cut-off frequencies by rationalizing the evenly spaced set (15),

$$\frac{m_i}{n_i} = \text{rationalize}\left(\frac{2a}{c} f_i, \varepsilon\right) \tag{18}$$

where m_i and n_i are a set of integers that give an approximately evenly spaced set of cut-off frequencies to within an error, ε. We should choose

$$\varepsilon < \frac{2a}{c}\Delta f \tag{19}$$

or the rationalization will return the same m and n for different values of i. However, making ε small requires large numerators (m_i) and denominators (n_i), and simulation time scales linearly with the number of unit cells, i.e. the denominator.

This issue of not being able to simulate any desired point in the parameter space is not unique to FDTD. This occurs in any method that attempts to simulate large or infinite problems with a finite volume and appropriate boundary conditions, and the problem possesses two or more indivisible spatial periods. In this case, simulations can only be performed for parameters that make all the spatial periods commensurate.

One spatial period in our problem is the wavelength of the field variation along the sample surface in the plane of incidence,

$$\lambda_x \equiv \frac{2\pi}{k_x} \tag{20}$$

This wavelength (which is twice the spacing between nodes of the port mode) must be commensurate with the other spatial period, the unit cell size, a,

$$l_x = m\frac{\lambda_x}{2} = na \tag{21}$$

4. FREQUENCY POINT SPACING

The spacing between the frequency points is determined by the length of the time series that is Fourier transformed. The time series can be extended arbitrarily by padding with zeros (truncation) or by use of an autoregressive (AR) filter to predict the long duration transient response of the system. The discrete Fourier transform of course returns points evenly spaced in frequency. Because the hyperbolic curves have steep slope near cut-off and are relatively flat near $f_{\max}$, this even spacing yields a much lower density of points in the f-$\sin\theta$ plane near cut-off. To obtain a desired point spacing in the $\sin\theta$ direction near cut-off, the following equation can be used,

$$N = \left(\frac{f_{\max}}{f_c} - 1\right)\frac{1}{\Delta_s} \tag{22}$$

where N is the number of frequency points, Δ_s is the spacing in the $\sin\theta$ direction near cut-off. However, this can lead to unnecessarily high point densities near $f_{\max}$, Figure 2. To keep the data sets smaller these points can be thinned to a more uniform density. This post simulation thinning may be necessary for the interpolation scheme described below.

Once we have the three parameter sets that will vary between simulations, m_i, n_i, N_i, the rest of the simulation model can be set up. Let the plane of incidence be the x–z plane, with the z-axis being normal to the sample surface, Figure 1. The simulation volume need have only one unit cell of metamaterial in the y-direction. It must have n_i unit cells in the x-direction and the same number of unit cells in the z-direction as the desired sample. The boundary conditions shown in the figure, (electric on the y-oriented faces, magnetic on the x-oriented faces and open on the z-oriented faces), are for S-polarization. P-polarization is obtained by swapping the electric and magnetic boundaries.

5. SIMULATIONS

The port mode numbers assigned by the simulation software may not be the same as the port mode number used here. MWS, for example, counts the uniform (normal incidence) mode as mode one, and assigns both TE and TM modes to the same numbering sequence according to their cut-off frequency. For S-polarization we wish to consider only the TE modes. This will generally not present a problem since the TE modes will have lower cut-offs than the TM modes due to the aspect ratio of our port, which is $1 \times n$, favouring the desired modes. Inclusion of an

x-oriented symmetry plane will decrease run times by a factor of two, but further complicates the mode number mapping.

If our unit cell lacks mirror plane symmetries in either transverse direction (x and y) then the extended sample being simulated may be different than what is expected. Electric and magnetic boundaries represent electric and magnetic mirrors which are not equivalent to periodic boundary conditions. Figure 3 gives two examples. When n is relatively large, the x-oriented boundaries result in a small number of reflections per unit length and will probably not affect the electromagnetic response much. However, whatever the impact, it will vary as n varies, which is undesirable. The y-oriented boundaries result in a reflection every cell, which will have significant impact on the response. This effect will at least be consistent across all simulations.

It is worth noting that the field orientation is fixed by the boundary conditions of the simulation and polarization rotation is not possible. This implies that the extended cell configurations resulting from the mirror boundary conditions are not bianisotropic or chiral, i.e. alternating ring orientation restores the missing mirror plane. To avoid all these symmetry issues and produce materials that are not bianisotropic or chiral, one can use a unit cell that is intrinsically symmetric, or use a symmetrized super unit cell made from two (or more) sub-cells.

Thick substrates present a problem because they create large non-periodic model spaces. These are best modelled as infinite substrates. This is accomplished by placing an open boundary directly on the substrate media block. In this configuration a port placed on this boundary will measure the fields propagating in the substrate rather than transmitted out of the substrate. Thus, the through sample transmission coefficient will not be available, though the reflection coefficient will be. When comparing to experiments, experimental results for

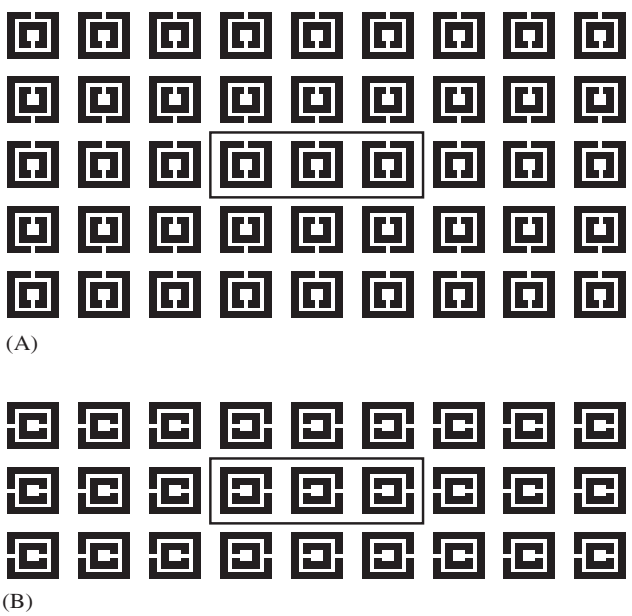

Figure 3. Extended cell configurations represented by a simulation model volume (shown enclosed in a rectangle) bounded by electric and magnetic boundary conditions.

the reflectivity of a thick substrate sample can be converted to effectively infinite substrate results by time gating techniques.

6. INTERPOLATION

After the simulations have run, we have data for S parameters on a set of points that cover the f-$\sin\theta$ parameter space. Unfortunately, this data set is not on a rectangular grid, so most plotting software cannot be used to create density or surface plots, nor can a simple reflectivity versus frequency at fixed angle (or reflectivity versus angle at fixed frequency) plot be generated without some interpolation.

A common interpolation scheme, used, for example, in making topographical maps, employs Delauney triangulation [18]. A Delauney triangulation is a list of connections between each point in a set and its nearest neighbours in the set (Figure 4). From these connections, one can easily find triangles that tile the parameter space and are useful for interpolations. If one wishes to know the value of the S parameter at a specific point, one finds the triangle which contains the point and then performs an interpolation of the three vertices of that triangle; we have used a linear interpolation, which effectively finds the plane passing through the three vertices.

The most technical part of this scheme, finding the connection lists is provided by common tools such as Mathematica and Matlab.

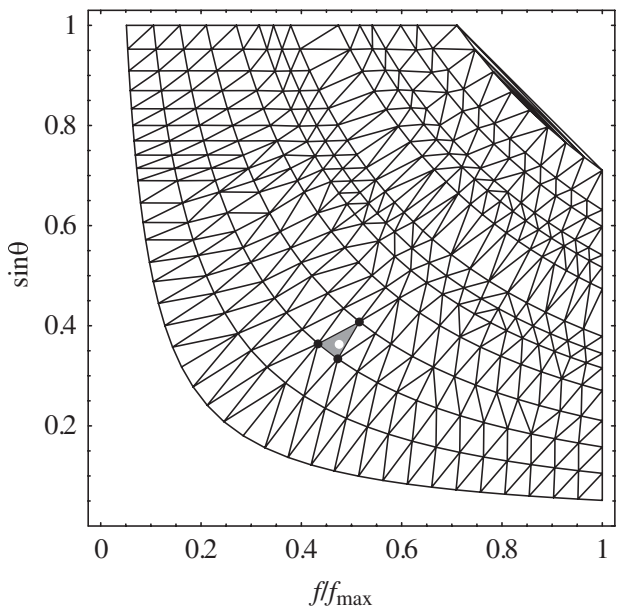

Figure 4. A sample DeLauney triangulation of a data set. To find the interpolated value of the white point, first find the triangle that contains it, shown shaded. Then interpolate the values at the vertices of that triangle, shown as black points. Note the irregular spacing of the hyperbolas which is typical when accommodating the lattice and mode spatial periods with reasonable rationalization.

To find the weights we proceed as follows. We solve the general equation for a plane passing through the three points (x_i, y_i, z_i)

$$\begin{vmatrix} x - x_1 & y - y_1 & z - z_1 \\ x_2 - x_1 & y_2 - y_1 & z_2 - z_1 \\ x_3 - x_1 & y_3 - y_1 & z_3 - z_1 \end{vmatrix} = 0 \tag{23}$$

for z, and put it in the form

$$z = \sum_{i=1}^{3} w_i(x, x_1, x_2, x_3, y, y_1, y_2, y_3) z_i \tag{24}$$

The coefficients, w_i are the desired weights. For our data, z_i and z are the complex valued S parameters at each of the vertices and the desired interpolated value, respectively. x_i, y_i, and x, y, are the real valued f and $\sin\theta$ of the vertices and the desired interpolation point, respectively. The weights, which must all be between zero and one, if the interpolation point is inside the triangle, can be used to determine if the containing triangle has been found or which of the three adjacent triangles is closer to the interpolation point. The closer of the three adjacent triangles is the one contiguous to the side joining the vertices with the largest weights. Using the weights in this way, one can move to continually closer triangles until the containing triangle is found.

Generating rectangular data for a plot usually involves interpolating closely space points along a line, in order. Thus, the containing triangle for the next point to be interpolated is usually the same or adjacent to, the last containing triangle. Storing the last containing triangle ensures that the search for the next containing triangle will usually take negligible time.

7. VALIDATION

We can test this method on a material with known analytical solution. We use a material with a unit cell that is homogenous and isotropic media with a resonant dielectric response of the Lorentzian form and unit magnetic permeability,

$$\varepsilon(\omega) = \varepsilon_\infty + \frac{(\varepsilon_0 - \varepsilon_\infty)\omega_0^2}{\omega_0^2 - \mathrm{i}\omega\gamma - \omega^2} \quad \text{and} \quad \mu = 1 \tag{25}$$

where $\varepsilon_\infty = 1$, $\varepsilon_0 = 3$, $\omega_0 = 2\pi(f_{\max}/2)$, and $\gamma = 0.5$. Our material will be one unit cell thick, where the lattice parameter is given by

$$a\frac{f_{\max}}{c} = \frac{2}{3} \tag{26}$$

The simulation results for the reflectivity, $|S_{11}|^2$, are plotted in Figure 5(A). Analytical results for this problem can be obtained using standard boundary matching techniques resulting in Fresnel formulas. The analytical results are shown in Figure 5(B). Figures 5(C) and (D) show excellent quantitative agreement between analytical results and the simulations for the reflectivity, $|S_{11}|^2$, and transmissivity, $|S_{21}|^2$, respectively. Over most of the domain the analytical and simulation curves are indistinguishable with a few glitches over small isolated regions.

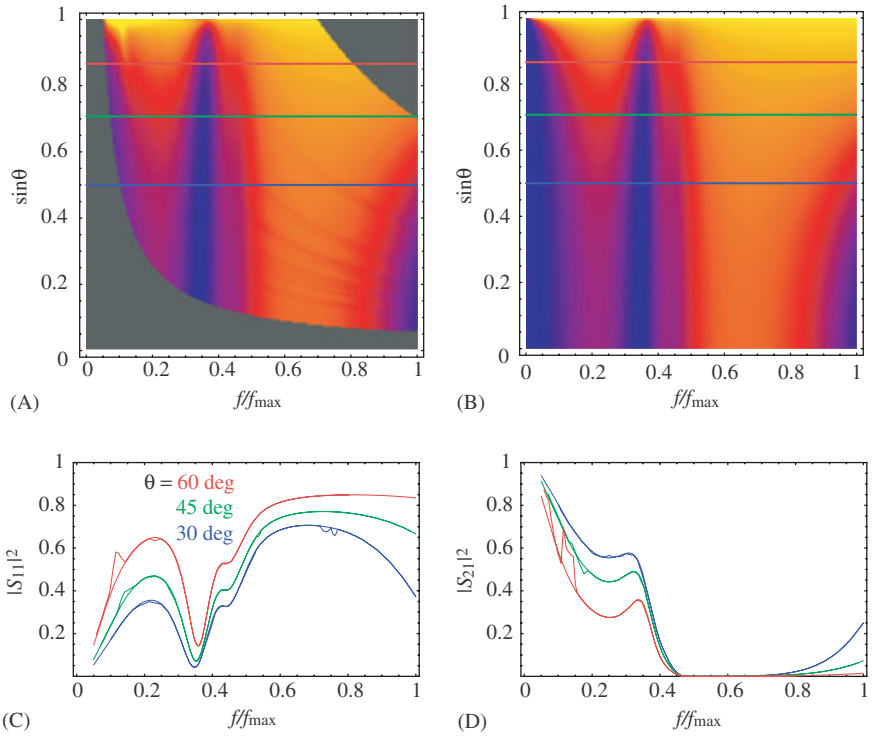

Figure 5. (A) Simulation results for reflectivity, $|S_{11}|^2$, of the test material; (B) shows the analytical results for the test material; and (C) and (D) compare the simulation and analytical results along constant angle lines in the data set for the reflectivity, $|S_{11}|^2$, and transmissivity, $|S_{21}|^2$, respectively.

8. SPLIT RINGS

We now show the method applied to a metamaterial. We have simulated the reflectivity, $|S_{11}|^2$, for a single layer of in-plane SRRs, Figure 6 (left). Here we have $a = 2.4$ mm and $f_{\max} = 20$ GHz, so that

$$a\frac{f_{\max}}{c} = 0.16 \tag{27}$$

We restrict ourselves to one ring orientation and polarization. Here we have chosen S-polarization and the orientation relative to the plane of incidence as shown in Figure 6(E). Note that the extended sample being simulated is as in Figure 3(A). We show the reflectivity versus frequency at a 30, 45 and 60° angle of incidence, Figure 6(C). Note that there is some slight artifact visible due to the hyperbolic curve shape of the data sets. Increasing the number of curves (and thus simulations) reduces this artifact, which is most visible where there are fine details in the reflectivity, such as at a narrow resonance.

An alternative to the direct calculation of the reflection at oblique angles of incidence is also shown in Figure 6 (right). Here we simulate the SRR structure for two orthogonal angles of incidence, (Figure 6(F)), and extract the (spatially local, bulk) material properties for these two

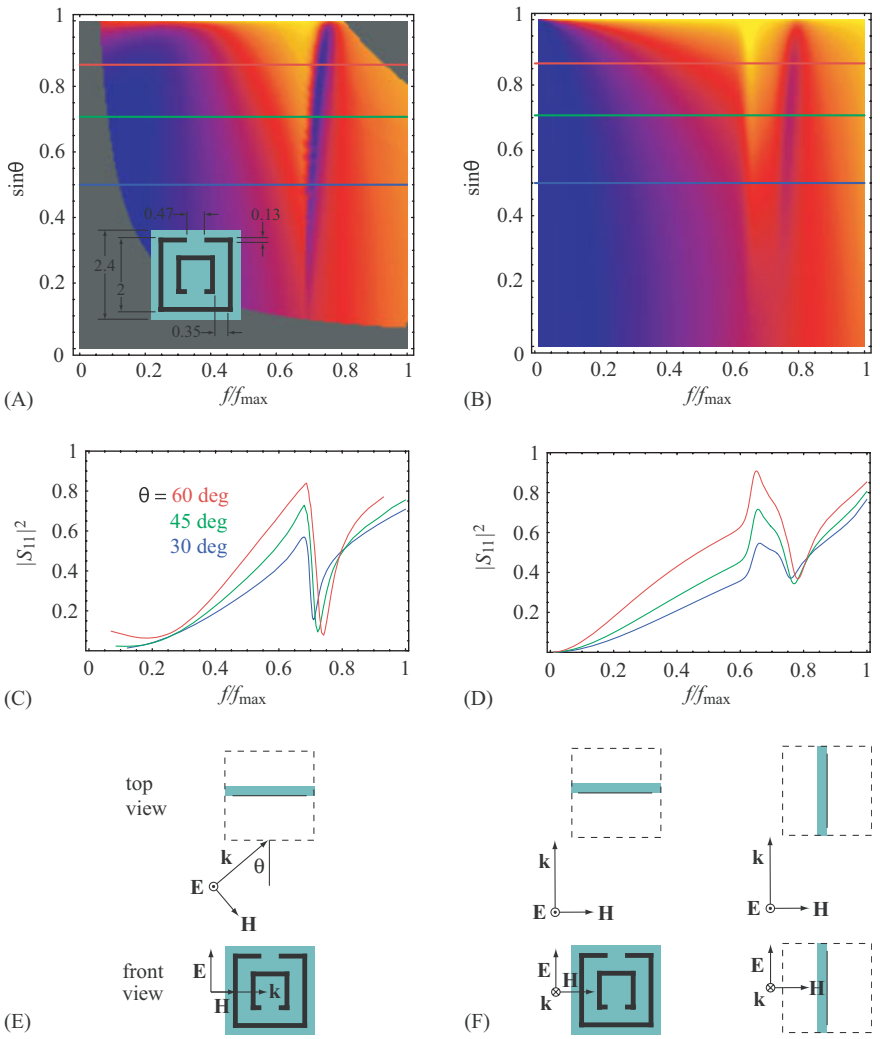

Figure 6. Simulation results for reflectivity ($|S_{11}|^2$) of a microwave SRR with S-polarization. $f_{max} = 20$ GHz: (A) shows the f-$\sin\theta$ parameter space for the direct oblique method; (B) shows the same results for an indirect numerical/analytical method described in the text; and (C) and (D) show the reflectivity versus frequency at fixed angle, corresponding to the horizontal lines in (A) and (B). The dimensions of the SRR in millimeters are given in the inset to (A). The substrate and metallization are 0.254 mm and 17 μm thick, respectively. The SRR orientations and polarizations are shown in (E) and (F).

orientations. Then using anisotropic Fresnel formulas we calculate the reflectivity at all angles. While there is qualitative agreement between the two methods, this latter method does not give good quantitative results. One reason for this is that the unit cell is only about six times smaller than the wavelength at the maximum frequency, so the media is somewhat spatially dispersive and spatially local material properties are not a perfect description. Secondly, a single layer of

unit cells does not behave exactly like thin bulk material since inter-cellular coupling is absent in the normal direction. Thus, good quantitative results for this single layer require the direct oblique method.

9. CONCLUSION

This method of simulating metamaterials with off-normal incident radiation is apparently accurate and applicable to metamaterials of interest. It should assist in the design and testing of future metamaterials and metamaterial devices.

ACKNOWLEDGEMENTS

I would like to acknowledge support from the IC Postdoctoral Fellowship Program and the Naval Air Warfare Center Weapons Division contract N68936-05-C-0011.

REFERENCES

1. Yen TJ, Padilla WJ, Fang N, Vier DC, Smith DR, Pendry JB, Basov DN, Zhang X. Terahertz magnetic response from artificial materials. *Science* 2004; **303**:1494–1496.
2. Linden S, Enkrich C, Wegener M, Zhou J, Koschny T, Soukoulis CM. Magnetic response of metamaterials at 100 terahertz. *Science* 2004; **306**:1351–1353.
3. Smith DR, Schurig D. Electromagnetic wave propagation in media with indefinite permittivity and permeability tensors. *Physics Review Letters* 2003; **90**:077405/1–4.
4. Marques R, Medina F, Rafii-El-Idriss R. Role of bianisotrophy in negative permeability and left-handed metamaterials. *Physics Review B* 2002; **65**:144440/1–6.
5. Padilla WJ. Unpublished, 2005.
6. Caloz C, Itoh T. Novel microwave devices and structures based on the transmission line approach of metamaterials. *Microwave Symposium Digest* 2003; **1**:195–198.
7. Fang N, Lee H, Sun C, Zhang X. Sub-diffraction-limited optical imaging with a silver superlens. *Science* 2005; **308**:534–537.
8. Schurig D, Smith DR. Negative index lens aberrations. *Physics Review E* 2004; **70**:065601(R)/1–4.
9. Weiland T, Schuhmann R, Greegor R, Parazzoli CG, Vetter AM, Smith DR, Vier DC, Schultz S. *Ab initio* numerical simulation of left-handed metamaterials: comparison of calculations and experiments. *Journal of Applied Physics* 2001; **90**:5419–5424.
10. Smith DR, Schultz S, Markos P, Soukoulis CM. Determination of effective permittivity and permeability of metamaterials from reflection and transmission coefficients. *Physics Review B* 2002; **65**:195104/1–5.
11. Ziolkowski R. Design, fabrication and testing of double negative metamaterials. *IEEE Transactions on Antennas and Propagation* 2003; **51**:1516–1529.
12. Smith DR, Padilla W, Vier DC, Nemat-Nasser SC, Schultz S. Composite medium with simultaneously negative permeability and permittivity. *Physics Review Letters* 2000; **84**:4184–4187.
13. Hannan P, Balfour M. Simulation of a phased-array antenna in waveguide. *IEEE Transactions on Antennas and Propagation* 1965; **13**:342–353.
14. Xin H, Kim M, Hacker J, Higgins J. Incident angle-dependent effective surface impedance (Zs) of electromagnetic crystal (EMXT). *IEEE Microwave and Wireless Components Letters* 2004; **14**:437–439.
15. Yang F, Rahmat-Samii Y. Reflection phase characterization of an electromagnetic band-ga (EBG) surface. *IEEE Antennas and Propagation Society: AP-S International Symposium* (*Digest*), vol. 3. 2002; 744–747.
16. Barlevy A, Rahmat-Samii Y. Characterization of electromagnetic band-gaps composed of multiple periodic tripods with interconnecting vias: concept, analysis and design. *IEEE Transactions on Antennas and Propagation* 2001; **49**:343–353.
17. Ramo S, Whinnery JR, Duzer TV. *Fields and Waves in Communication Electronics* (3rd edn). Wiley: New York, 1994.
18. DF W, Phillip G. Triangle based interpolation. *Mathematical Geology* 1984; **8**:779–795.

AUTHOR'S BIOGRAPHY

David Schurig was born in the 1960's in Burbank, California. He received his BS in Engineering Physics from U.C. Berkeley, and then worked at Lawrence Berkeley Lab on laser ablation and photoacoustic spectroscopy. Later, he enrolled in graduate school. After performing many unpublished experiments, David submitted a theoretical thesis on *negative index media*, the *perfect lens* and related structures to his committee. In exchange, U.C. San Diego granted him a PhD in physics in 2002. In the early part of the new millennium David also worked for the California Space Institute, performing space mission feasibility studies, and for Tristan Technologies (named after the coldest, continuously inhabited place on earth), designing and building, cryogenically cooled, SQUID-based instruments. David is now a post doctoral fellow at Duke University in Durham, North Carolina, where there are seasons. He is designing metamaterials and lens antennas and other structures made from metamaterials.